atmosphere

MDPI

Article

Examination of the Influence of Alternative Fuels on Particulate Matter Properties Emitted from a Non-Proprietary Combustor

Liam D. Smith [1], Joseph Harper [2], Eliot Durand [2], Andrew Crayford [2], Mark Johnson [3], Hugh Coe [1] and Paul I. Williams [1,4,*]

[1] School of Natural Sciences, University of Manchester, Manchester M13 9PL, UK; liamsmith957@gmail.com (L.D.S.)
[2] Cardiff School of Engineering, Cardiff University, Cardiff CF24 3AA, UK; harperj4@cardiff.ac.uk (J.H.); durandef@cardiff.ac.uk (E.D.); crayfordap1@cardiff.ac.uk (A.C.)
[3] Rolls-Royce, plc, Sin A-37 PO Box 31, Derby DE24 8BJ, UK
[4] National Centre for Atmospheric Science, Leeds LS2 9PH, UK
* Correspondence: paul.i.williams@manchester.ac.uk

Abstract: The aviation sector, like most other sectors, is moving towards becoming net zero. In the medium to long term, this will mean an increase in the use of sustainable aviation fuels. Research exists on the impact of fuel composition on non-volatile particulate matter (nvPM) emissions. However, there is more sparsity when considering the impact on volatile particulate matter (vPM) emissions. Here, nine different fuels were tested using an open-source design combustor rig. An aerosol mass spectrometer (AMS) was used to examine the mass-loading and composition of vPM, with a simple linear regression algorithm used to compare relative mass spectrum similarity. The diaromatic, cycloalkane and aromatic contents of the fuels were observed to correlate with the measured total number concentration and nvPM mass concentrations, resulting in an inverse correlation with increasing hydrogen content. The impacts of fuel properties on other physical properties within the combustion process and how they might impact the particulate matter (PM) are considered for future research. Unlike previous studies, fuel had a very limited impact on the organic aerosol's composition at the combustor exit measurement location. Using a novel combination of Positive Matrix Factorization (PMF) and high-resolution AMS analysis, new insight has been provided into the organic composition. Both the alkane organic aerosol (AlkOA) and quenched organic aerosol (QOA) factors contained C_nH_{2n+1}, C_nH_{2n-1} and C_nH_{2n} ion series, implying alkanes and alkenes in both, and approximately 12% oxygenated species in the QOA factor. These results highlight the emerging differences in the vPM compositional data observed between combustor rigs and full engines.

Keywords: aircraft; aerosol; fuel; engine; particulate matter

Citation: Smith, L.D.; Harper, J.; Durand, E.; Crayford, A.; Johnson, M.; Coe, H.; Williams, P.I. Examination of the Influence of Alternative Fuels on Particulate Matter Properties Emitted from a Non-Proprietary Combustor. *Atmosphere* **2024**, *15*, 308. https://doi.org/10.3390/atmos15030308

Academic Editor: Georgios Karavalakis

Received: 19 January 2024
Revised: 14 February 2024
Accepted: 20 February 2024
Published: 29 February 2024

1. Introduction

Global air travel is set to increase annually at a rate of 5% per year [1]. Without mitigation, the emissions produced by the aviation sector will subsequently increase year on year [2]. Aircraft engines emit a complex mixture of gases and particulate matter (PM) which impact both the climate [3] and local air quality [4,5]. The latter is linked to increases in premature death resulting from air degradation surrounding airports [6]. Aviation gas turbine engine PM has also been related to toxicity in exposed human bronchial cells [7]. Aviation PM is generally classed as either non-volatile PM (nvPM), formed from combustion products, or volatile PM (vPM), formed from condensed species originating from the engine's fuel and sometimes its lubrication oil [8]. Engine performance data are often restricted due to intellectual property protections, meaning linking emission characteristics to engine technologies is not always possible.

The aviation sector is dependent on fossil fuels, but with the industry's carbon neutral goal outlined on Flight 2050 and individual country's goals to be carbon neutral no later

than 2050, the sector is looking at alternative technologies and fuels to meet this target. One of those solutions is adoption of sustainable alternative fuels. The composition of fuel has been shown to impact the nvPM emissions, with increased hydrogen content, via a reduction in aromatics, leading to lower nvPM emissions; however, the naphthalenic content of the fuel has also been shown to be disproportionate in its effect on the magnitude of the non-volatile number and mass emission index (EI) [9–12]. Conversely, it has been shown that an increased fuel sulphur content results in higher sulphate mass concentration [13–15] and nucleation mode particles [12,16–18] in the plume of the aviation emission sources. Several dedicated research campaigns—such as the APEX [19], AAFEX-I [16,20] and AAFEX-II [21] campaigns—have examined aviation fuel properties and their relationship with PM emissions. These are the most extensive contributions to the field to-date. However, due to their use of a single engine type (CFM56-2C1), large operating costs and the influence of atmospheric conditions on the evolving plume measurements (due to their large sampling distances), they are difficult to replicate for both future comparisons and routine evaluations of new fuel types. Moreover, while the use of full engines is more accurate for the assessment of in situ impacts of a given fuel, this introduces uncertainty for future fuel comparisons due to the proprietary nature of the engine operating conditions. Therefore, this study aims to examine how changing fuel properties govern PM emissions on an aviation-relevant open-sourced design combustor rig, measured using an International Civil Aviation Organization (ICAO) compliant sampling system.

This study was performed at Cardiff University's Gas Turbine Research Centre (GTRC), as part of the JetSCREEN (JET fuel SCREENing and optimisation platform for alternative fuels) campaign. Nine aviation fuels were tested, with the aim of examining the relationship between fuel composition and emitted nvPM number and mass concentrations, measured by Cardiff University. Additional characterisation of vPM was undertaken by the University of Manchester, to examine the total aerosol number concentration, non-volatile and volatile mass concentrations and volatile PM composition. This was achieved using the standardised European Union Aviation Safety Agency's (EASA) aircraft engine nvPM sampling system alongside a range of aerosol science instrumentation, which has been previously demonstrated on jet engines [22–25].

2. Materials and Methods

2.1. Fuels

Details of the nine fuels tested are presented in Table 1 and Figure 1. Three conventional Jet A-1 fuels (J-REF, J-LA and J-HA), two SAF (A-LA and A-HA) and four blends (B-REF, B-HE1, B-HE2 and B-HA) were tested. J-REF was a typical Jet A-1 fuel and was used as the reference fuel for this study, J-HA was a high aromatic Jet A-1 with reduced sulphur content and J-LA was a lower aromatic Jet A-1 with high naphthalenes and with near-zero sulphur and reduced diaromatics relative to J-REF. The SAFs consisted of A-LA, an Alcohol-to-Jet synthetic paraffinic kerosene (ATJ-SPK), with a composition entirely of alkanes, and A-HA, a Catalytic Hydrothermal Conversion Jet (CHCJ) fuel, possessing the highest total aromatic content of the fuels examined, with relatively low naphthalene content. Finally, four fuel blends of conventional fuel and SAF fuels were examined. B-REF was 70% J-REF and 30% A-LA volumetrically. The other three blends (B-HE1, B-HE2 and B-HA) contained a HEFA fuel with a very high alkane content and low aromatic content. B-HE1 was 51% J-HA and 49% HEFA volumetrically, while B-HE2 was 70% J-LA and 30% HEFA, exhibiting a similar total aromatic content but lower di-aromatics. B-HA was 49% J-HA, 34% J-LA and 17% HEFA and had the highest aromatic content of the fuel blends tested.

Table 1. An overview of the fuels examined in this study.

Fuel	J-REF	J-HA	J-LA	B-REF	B-HE1	B-HE2	B-HA	A-HA	A-LA
Hydrogen Mass (%)	14.022 (±0.024)	13.649 (±0.046)	14.083 (±0.029)	14.405 (±0.006)	14.397 (±0.074)	14.514 (±0.036)	14.042 (±0.033)	13.510 (±0.007)	15.31 (±0.003)
Alkane Content (%)	49.96	37.83	49.47	76.83	63.42	62.72	49.64	28.86	99.90
Monoaromatic Content (%)	18.41	20.57	17.82	12.89	11.48	12.68	16.61	24.91	0.00
Diaromatic Content (%)	1.82	2.18	0.18	1.28	1.22	0.14	1.26	0.28	0.00
Weight Total Aromatic Content (%)	20.24	22.75	18.01	14.16	12.7	12.82	17.87	25.18	0.00
Sulphur Content (ppm)	200	105	5.7	140	56.8	4.10	58.6	0.00	0.00
Molecular Weight (g/mol)	153.6	162.37	151.64	181.55	166.92	156.00	159.89	159.82	200.17
Kinematic viscosity (mm^2/s)	1.62	1.62	1.3	1.64	1.59	1.39	1.57	1.72	1.74
Surface Tension (mn/m)	25.9	27	25.67	25.07	25.63	25.23	26.13	27.60	27.00

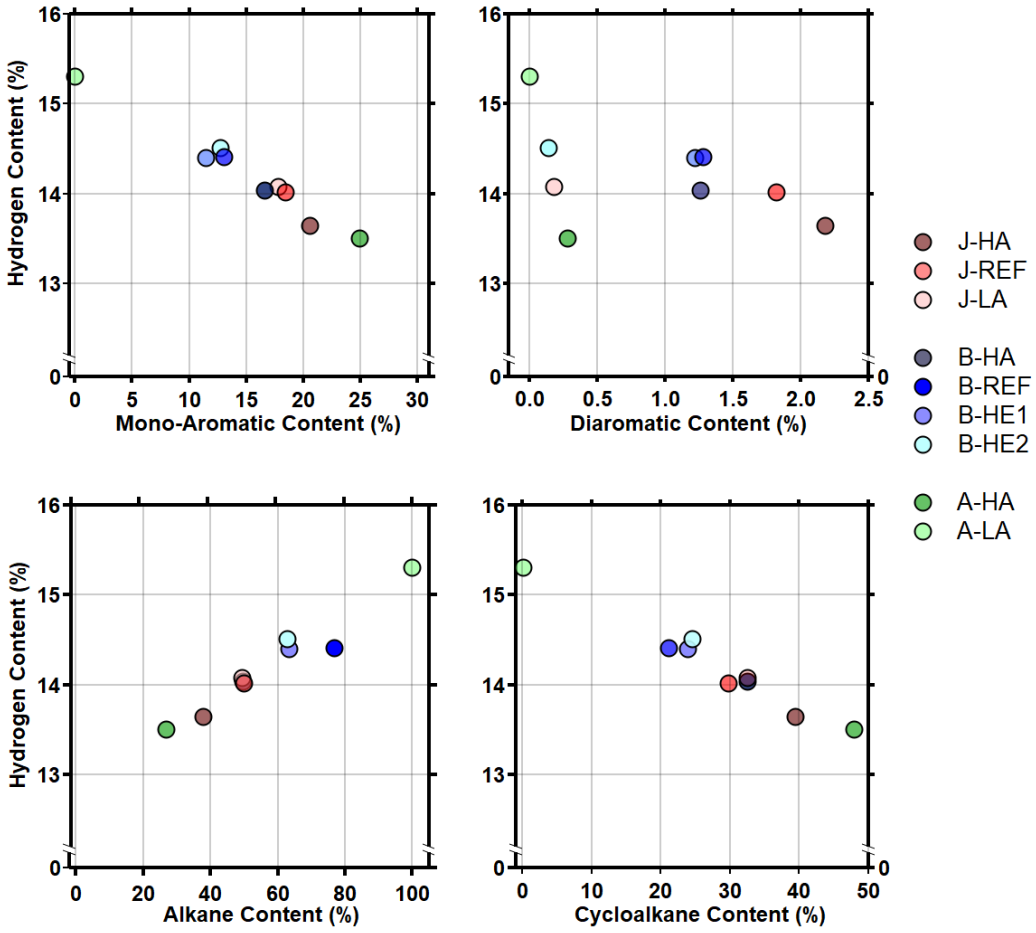

Figure 1. Hydrogen content versus alkane, mono-aromatic and cycloalkane content of the nine fuels examined.

Descriptions of the analysis techniques used to determine fuel properties are described further in Harper et al., 2022 [9]. In short, the compositional analysis was undertaken using 2D-GCxGC for all fuels. Here, mono-aromatic compounds are classified as any molecule which contains a single aromatic ring, while di-aromatics contain two aromatic rings. Polyaromatics (i.e., compounds containing three or more aromatic rings) were negligible across all the fuels tested. Across the fuels examined, a greater proportion of alkane mass was inversely associated with the proportion of the fuel's cycloalkane and monoaromatic content. This compositional shift to a greater alkane content resulted in a higher proportion

of hydrogen, and thus a higher H:C ratio. Diaromatics varied somewhat independently from these (Figure 1).

2.2. Combustor

The combustor used in this study, only briefly described here, utilises an open-source design allowing for combustor emission model development and validation. The combustor rig's design is described fully by Harper et al. [9] and is based on a single rich-quench-lean (RQL) scaled combustor can proposed by Makida et al., 2006 [26]. In the configuration used for this study, 10 mm and 8 mm primary and secondary quench air supplies were used. Fuel was delivered to the combustor using a pre-filming air-blast atomiser, which followed a Parker–Hannifin design, as described in Crayford et al., 2019 [27]. The combustor was housed in a generic high-pressure optical chamber (HPOC). Fuel and air, heated to 30 °C and 80 °C, respectively, were supplied to the atomiser independently and independently varied to control the local AFR in the primary 'rich-zone'. Secondary 'quench' air was pre-heated to 120 °C and delivered into the HPOC before entering the combustor liner via the differential pressure across it. The preheating was conducted to eliminate uncertainties associated with flow behaviours and fuel physical properties due to day-to-day variability in ambient conditions, whilst also standardising the observed pressure drops across the atomiser and liner.

2.3. Setup and Sampling

An ICAO compliant sampling and measurement system [28] was used to extract and quantify the aerosol, a schematic of which is shown in Figure 2. In this study, the European reference system was used, which is co-owned by the European Aviation Safety Agency and Cardiff University, who are responsible for its operation. In addition to regulatory nvPM and gaseous measurements, several previous studies have used this sampling system to also sample vPM [23,25].

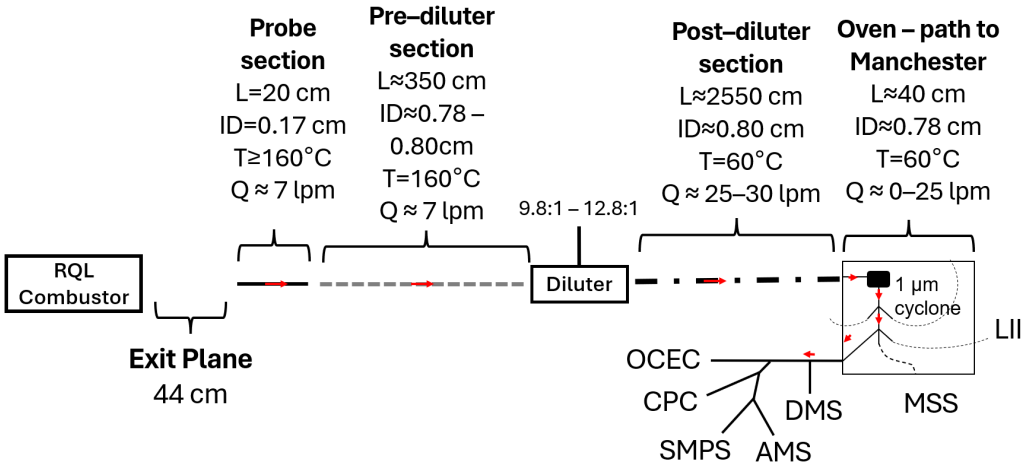

Figure 2. Schematic of experimental setup. Note: nvPM number instrumentation and catalytic stripper described in text are not shown here for clarity as the results from these are not presented.

The sample was captured via a 9-point equal area "piccolo" exhaust probe, located 0.44 m downstream of the combustor exit. The sample was then diluted using a Dekati VKL-10 eductor diluter, which exhibited a range of compliant dilution ratios dependant on operating conditions (9.8–12.8:1). All values presented in this study are dilution corrected unless otherwise stated.

The dilution air supplied to the diluter shown in Figure 2 was HEPA filtered, and cleanliness checks were performed on the full nvPM system. Post-dilution exhaust sample was then transported via a 25 m heated Winkler (WAKG) sampling line and bespoke heated splitter oven, each maintaining the sample at 60 °C. The conditioned sample then entered the nvPM mass and the nvPM number instrumentation, the latter of which had an inbuilt

catalytic stripper (CS), to ensure any nucleated volatiles were not counted. A DMS-500 measured additional nvPM size distributions. A third split from the oven supplied the University of Manchester's aerosol instrumentation, via a 1 m long, ¼" OD stainless steel line, as discussed further in Section 2.4.

2.4. Instrumentation

As discussed previously, the PM emitted from gas turbine engines is often separated into two categories: nvPM and vPM. The term nvPM is standardised for PM aircraft regulation, referring to solid particles at the engine exit plane which do not volatilise at temperatures up to 350 °C [28]. Meanwhile, vPM is not a standardised term but is defined in the scientific literature as PM that forms outside of the combustor and volatilises at temperatures less than or equal to 350 °C [29]. A range of instruments were utilised to examine both PM types, which are displayed in Table 2. A brief description of the instrumentation is presented here, but a more detailed description is available in Smith et al. (2022) [25], where, with the exception of MSS, the same instrumentation was applied.

Table 2. Instrumentation used in this paper.

Instrument	Species Measured	Unit of Measurement	Detection Limits	Time Resolution
CPC [a]	Total Number Concentration	Number/cm^3	2.5 nm–2–3 µm	1 s
SMPS [b]	Size Distribution	$dN/dlogD_p$	8 nm–150 nm	Full Scan ~2.5 min
OCEC Analyser [c]	Organic Carbon and Elemental Carbon	µg/m^3	N/A	User-specified sample time (in this study, always between 30 and 60 min), with user-specified analysis protocol [d]
HR-AMS [e]	Non-Refractory Aerosol Species [f]	µg/m^3	~30 nm–1 µm [g]	Full Scan 30 s
MSS and LII [h]	Refractory Black Carbon (rBC), converted to Elemental Carbon	µg/m^3	~1 µg/m^3	1 Hz (MSS) and 20 Hz (LII)

[a] Condensation Particle Counter, model 3776 (TSI). [b] Scanning Mobility Particle Sizer, model 3077 (TSI), equipped with a CPC model 3776 (TSI) for classification. [c] Sunset Organic Carbon Elemental Carbon (OCEC) Analyser. [d] Sample times were altered depending on concentrations. However, mass concentrations presented are normalised for comparison. In this study, a modified NIOSH 5040 protocol was applied. [e] High-Resolution Aerosol Mass Spectrometer (HR-AMS) (Aerodyne). [f] Aerosol that is vaporised at 600 °C under vacuum conditions; this includes organics, sulphate, nitrate, ammonia and chlorine. [g] 50% of particles are lost at 30 nm and 1 µm, with a steep drop in detection in particles smaller and greater than these sizes, respectively. [h] AVL Micro Soot Sensor (MSS) and Artium Laser-Induced Incandescence (LII 300, referred to as LII for brevity).

As discussed, the ICAO-compliant European nvPM system was used to provide the nvPM number and mass concentrations using mobile instrumentation located at the end of the sampling lines. Mass concentrations of nvPM were measured using an AVL Micro Soot Sensor (MSS) and a Laser-Induced Incandescence soot instrument (LII 300; referred to here as the LII), with an AVL Advanced Particle Counter (APC) used for nvPM number concentrations.

The University of Manchester's equipment included the following instruments: a TSI 3776 Condensation Particle Counter (CPC; particle number concentration), Scanning Mobility Particle Sizer (SMPS with 3085 nano DMA and 3776 CPC; particle size distribution), Sunset Organic Carbon Elemental Carbon (OCEC) Analyser and Aerodyne High-Resolution Time-of-Flight Aerosol Mass Spectrometer (HR-ToF-AMS; referred to as AMS for brevity; non-refractory chemical composition). Every size distribution taken on the SMPS from this paper is displayed in Figure S4.

As the CPC and SMPS are commercially available equipment, their operation is not described here as information is widely available. The total number CPC and the CPC

used for the SMPS were intercompared for size-dependent concentrations. Both CPCs compared well (R^2 = 0.9995; Figure S1). The total number CPC was over-range for most of the test points, so SMPS-integrated total number concentrations are reported in these results, and any mention of total particle concentrations thus refers to the SMPS total concentrations. For validation, the SMPS' total number concentrations were compared against the CPC's while it was in single particle count mode (concentrations < 3×10^5), offering good corelation (R^2 = 0.91; Figure S1b). However, it is observed that there is a bias between the counts, with the SMPS typically reporting concentrations circa 50% lower than that of the CPC. The high-resolution AMS used here provides better unit mass resolution, enabling the differentiation of specific ions detected by the instrument at a given mass to charge ratio (*m/z*). This provides the ability to differentiate between purely hydrocarbon and oxygenated ions from the emitted aerosol, allowing for greater understanding of aerosol composition. The analysis of AMS data is discussed further in Section 2.7.

The OCEC analyser, including its usage and protocol, is described in greater detail in Smith et al. (2022) [25]. For clarity of results, the reader should note that the OCEC is a semi-continuous instrument, meaning that it draws a sample of aerosol laden sample for a user-designated length of time, depositing the aerosol onto a quartz filter. Once complete, the inlet is sealed, and the instrument then undergoes a period of analysing the sample (because of this, OCEC data collection was possible on only one test point—Test Point 8—in which the combustor was held at the condition for 30–60 min. After sampling, the analysis involves exposing the deposited aerosol to two different gas mixtures, the first being an oxygen-free helium gas (to examine OC) and later a 90% helium and 10% oxygen mixture (to examine EC). The deposited sample in both atmospheres is progressively heated up to convert the carbon species to CO_2 in temperatures and durations chosen by the user. The OCEC in this study used an altered NIOSH5040 analysis protocol, the details of which are included in Table S1.

In the graphs presented, where an average is taken, the error bars are the standard deviation, with the exception of the boxplots which show the top and bottom quartiles (i.e., indicate the full range of observations). For single-point measurements of some instruments (the OCEC, SMPS and, in some instances, AMS, due to the short run times and longer scan times), error is the measurement uncertainty. For the SMPS GMD, this is ±10%, the AMS ±30% and the OCEC ±10%.

2.5. Line Loss Correction

Particles measured via any sampling system are subject to line losses through numerous mechanisms (e.g., diffusion, inertia, thermophoresis, etc.); therefore, accurately relating measured concentrations (at the end of the sampling system) to real-world engine exit emissions requires line loss corrections [30]. Although the size distributions in this study (Figure S2) typically ranged from 20–30 nm, leading to differences in experienced size-dependent system loss and, hence, accuracy in approximating combustor outlet PM concentrations.

Using an almost identical experimental configuration, Harper et al., 2022 [9] calculated that the nvPM number reductions witnessed for the cleanest (highest hydrogen content) SAFs were overreported by ~6%, due to the relatively higher particle losses of the smaller particles witnessed for these fuels. However, it was noted that a reduced impact was observed in the case of mass concentration, as this is dominated by the larger particles of any given number weighted size distribution. In light of this observation, given this work is primarily focused on mass and chemical composition, line loss correction was not deemed necessary for this study, given line loss correction does not change the vPM composition data.

2.6. Test Matrix

For each fuel, the combustor rig ran through a range of conditions across five operating metrics: fuel flow rate, primary air flow rate, secondary air flow rate, primary air-to-fuel

ratio and global air-to-fuel ratio (AFR). The conditions were named as eight test points (TP) and are presented in Table 3. For all fuels, the rig ran at TP1–7 for only ~3 min, and during TP8 it was held at a stable condition for 30–60 min, with almost 100% data coverage (exceptions being J-HA's TP4 and 5). The data presented here, are frequently averaged across several TPs on a given fuel. When J-HA is included in the analysis, all fuels are only averaged across TP1–3 and TP6–8 to ensure compatibility, unless otherwise stated. One notable exception is for total number concentrations, in which averages across TP1–3 and TP6–7 are presented due to instrument failure on J-LA's TP8.

Table 3. Rig operating conditions used in this research.

Test Point (TP)	Fuel Flow (g/s)	Primary Air (g/s)	Secondary Air (g/s)	Primary Air-to-Fuel Ratio	Global Air-to-Fuel Ratio
1	0.8	2.42	25	3.03	34.28
2	0.7	2.42	30	3.46	46.31
3	0.6	2.42	30	4.03	54.03
4	0.6	2.42	25	4.03	45.70
5	0.6	2.07	30	3.45	53.45
6	0.7	2.07	30	2.96	45.81
7	0.8	2.07	25	2.59	33.84
8	0.6	2.07	35	3.45	61.78

2.7. AMS Data Analysis

AMS data were processed in IGOR 6.37, using the ToF-AMS data analysis software SQUIRREL v1.57H, alongside the PIKA toolkit for the high-resolution AMS data. As part of the data processing, to remove gas contributions to the aerosol mass spectra detected by the AMS, test point-specific corrections were applied. Gas contribution was measured by diverting the AMS's flow through a HEPA filter at each test point. Ratios of detected gases relative to the N_2 were taken at each test point and applied in the SQUIRREL toolkit's frag table, which then subtracted each gas's contribution from the normal AMS scan. Figures S3 and S4 show a comparison of the SQUIRREL vs. PIKA and residuals from the PIKA analysis, respectively.

AMS mass spectra were analysed further using Positive Matrix Factorisation (PMF). PMF has been previously used to examine aircraft engine and combustor emissions [25,31]. The methodology applied in this manuscript is described in full in Smith et al., 2022 [25]. Briefly, the organic mass spectra are broken down into a series of contributing factors. The number of factors is user definable, with a factor solution chosen with the aim of reducing the Q/Qexp value to as close to one as possible. The chosen factor is then validated with good external instrument tracer correlations whilst maintaining physical plausibility of each factor's mass spectrum. The aim of reducing the Q/Qexp value came with the caveat of not reducing the strength identified tracer correlations. Solutions between one and five factors were examined. Factor splitting above three factors was investigated,. with a three-factor solution improving the Q/Qexp relative to the two-factor solution, but it was observed that the third factor only contained a single mass at *m/z* 44 and marginally decreased the regression coefficients of the other factors when plotted against instrument tracers. Because of this finding, a two-factor solution was ultimately applied to these data.

3. Results

3.1. Instrument Comparisons

A comparison of the instrument data is shown in Figure 3. The total number concentration can be seen to be increasing with the purely non-volatile mass (both the OCEC and MSS EC mass (Figure 3A)) and the sum of volatile and non-volatile mass shown in Figure 3B by the OCEC-detected TC and the sum of MSS EC and AMS organic mass concentrations. Similar to Figure 3A, the total number increases with increasing total detected mass, which

implies the majority of vPM is condensed on the nvPM surface as the addition of organic matter does little to affect the trend. The OCEC analyser EC mass concentrations and MSS nvPM mass concentrations were also in good agreement (Figure 3C; R^2 = 0.87) for all fuel's at TP8.

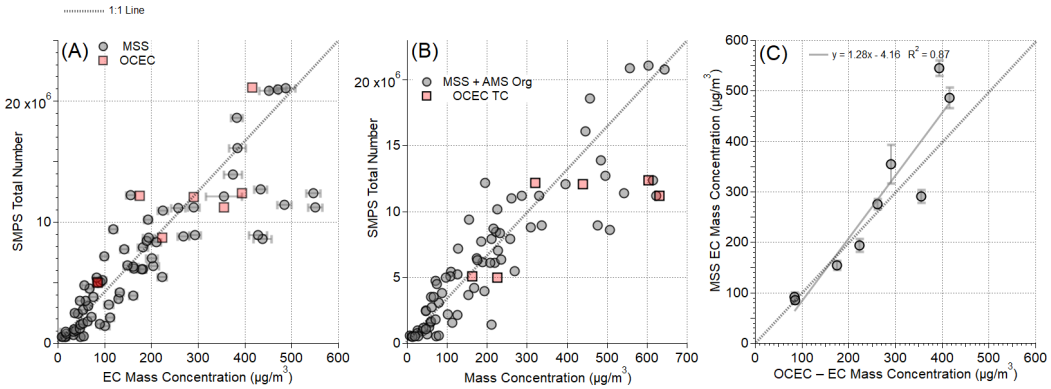

Figure 3. Comparison of different instrument measurements (**A**)—number concentrations versus EC mass concentration, (**B**)—number concentrations versus TC and EC mass concentrations, (**C**)—EC mass concentrations) from several different aerosol instruments. Error bars show one standard deviation. The 1:1 line is shown in all graphs.

3.2. Total Particle Number Concentrations

The total number concentrations decreased with increasing fuel hydrogen content, possessing the strongest correlation between emissions and fuel properties considered for this study (Figure S10). The averaging across all conditions for a given fuel flow rate is shown in Figure 4A and Table S2. Generally, with higher fuel flow rates and lower global AFRs, the particle number concentrations were lower, but the importance of increased fuel hydrogen content is still seen.

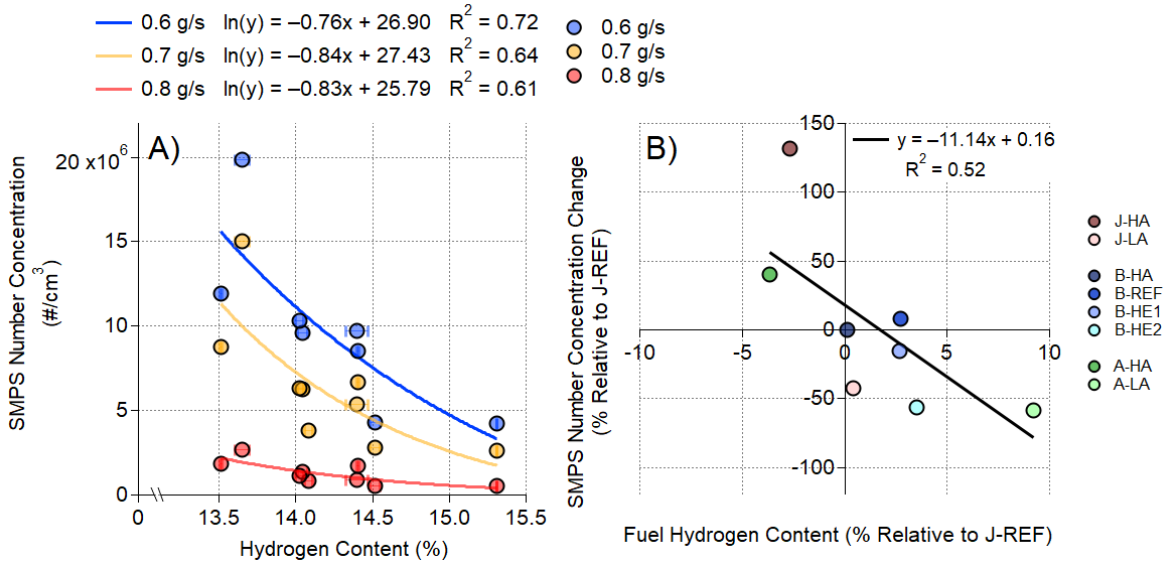

Figure 4. Particle number concentrations (**A**) as a function of fuel hydrogen content, averaged across a given fuel flow rate, whilst other variables were changing (for all other variables held constant, see Figure S5). In (**B**), relative differences in hydrogen content and number concentrations are presented, the latter of which is averaged across all conditions (T1–T3 and T6–T7; excluded test points are as such due to SMPS failure for J-LA's TP8 and J-HA's lack of TP4–5). Values in 4b are compared against those of J-REF. X-axis error bars in 4a show one standard deviation for fuel's repeatability of their compositional analysis. Y error bars are not shown but are SMPS measurement uncertainty (±10%). Regression values are results of linear regression with the natural log of displayed y values.

Relative to J-REF, when averaged across all test points (excluding T4 and T5, to allow inclusion of J-HA and A-HA, which had no data at these points), the number concentrations increased between 40 and 132% in the fuels with lower hydrogen content (Figure 4B). The greatest reduction from hydrogen increase was seen from A-LA—which possessed 9% greater hydrogen—with a 58% reduction in average particle number concentrations. B-HE2 saw a similar decrease of 57%, while having just a 3.5% greater hydrogen content.

As shown in Figure 1, monoaromatics and cycloalkanes do not vary independently with hydrogen content, so their relative importance over hydrogen content could not be determined. Diaromatics, however, did vary more independently from hydrogen content (Figure 1) and correlated with particle number concentrations (R^2 = 0.5 when averaged across TP1–3 and TP6–7, Figure S10). The fuel's molecular weight also varied independently from diaromatics but correlated moderately well with cycloalkanes (R^2 = 0.61) and monoaromatics (R^2 = 0.63). Viscosity also did not correlate with hydrogen content (R^2 = 0.005). Because molecular weight, diaromatics and viscosity varied independently from hydrogen content, monoaromatic and cycloalkane content, their relative importance can be more easily analysed. The importance of the fuel composition not captured through hydrogen content is discussed further in the Section 4.

3.3. nvPM Mass Concentrations

The nvPM mass concentration trends when averaged across all conditions for a given fuel flow rate were similar to those reported for the total PM number concentrations, decreasing with increasing fuel flow (and hence decreasing global AFR) (Figure 5A. Again, hydrogen content was the individual fuel metric with the strongest correlation (Figure S11). The average nvPM mass concentration changes for each fuel relative to J-REF at each fuel flow are shown in Table S3. The change relative to J-REF ranged from +176% to –75% across the other fuels examined. A-LA exhibited the greatest average reduction at every fuel flow. The only fuels with lower hydrogen relative to J-REF—J-HA and A-HA—had a 124 and 163% higher average EC mass concentration than J-REF, respectively. The inverse was true for the fuel's average number concentration reductions relative to J-REF, as J-HA had a higher increase in total number (132%, relative to J-REF) than A-HA (40%, relative to J-REF), despite A-HA's higher reductions in EC mass.

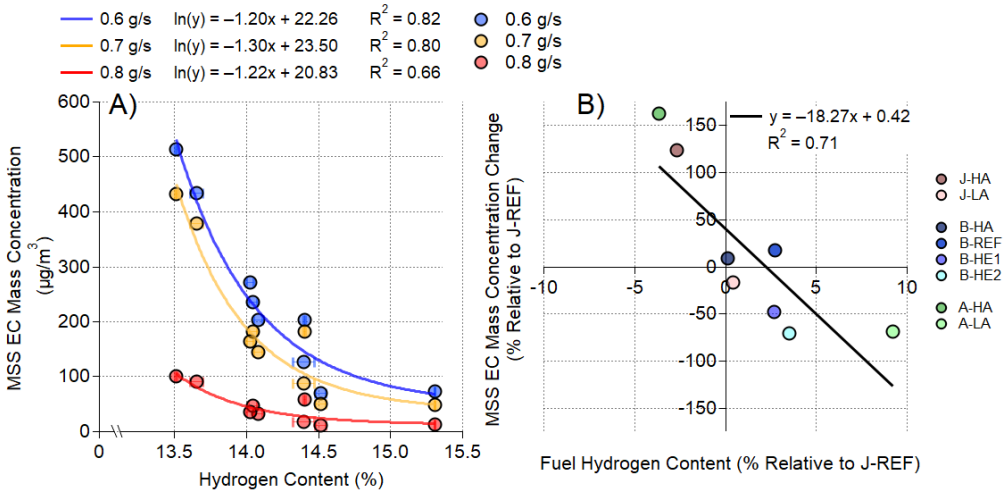

Figure 5. nvPM mass concentrations (**A**) as a function of fuel hydrogen content, averaged across a given fuel flow rate, whilst other variables are changing (for all other variables held constant, see Figure S5). In (**B**), relative differences of hydrogen content and nvPM mass concentrations are presented, the latter of which is averaged across all conditions (T1–T3 and T6–T7). Both values are compared against those of J-REF. X-axis error bars in 5a show one standard deviation for fuel's repeatability of their compositional analysis. Regression values are results of linear regression with the natural log of displayed y values.

3.4. vPM

Sulphate was not seen in great quantities and appeared to be around the limit of detection for all fuels and conditions tested.

The vPM observed here therefore consisted entirely of organic material. The detected organics correlate well with EC mass concentrations. The AMS organics correlated with MSS mass concentrations (Figure S6; $R^2 = 0.76$) and the OCEC-detected OC correlated with the OCEC-detected EC (Figure S7; with one anomaly—B-REF—removed: $R^2 = 0.66$).

To examine if organic vPM composition changed as a function of fuel composition, ordinary least squares (OLS) linear regression was performed on the 70 mass spectra observed in this study, resulting in 235 mass spectral comparisons and linear regressions. The organic mass concentration produced at each *m/z* (up to *m/z* 150) by a fuel at a given condition was compared against the equivalent *m/z* of the organic vPM emitted by another fuel at the same operating condition. To obtain a good signal to noise ratio, different organic mass concentration thresholds were applied ensuring good data quality. The results of this are shown in Table S4. An organic mass concentration threshold of 0.5 $\mu g/m^3$ was chosen, as this provided the largest decrease in standard deviation whilst retaining most (66 of mass spectra, 93% of those collected) of the comparisons. This value is above the instrument's limit of detection threshold for mass concentrations, providing more signal to noise. All data shown in Figure 6 involve conditions above this threshold, with conditions below this threshold not compared (with no threshold, using all 70 mass spectra, there were 272 comparisons). *m/z* 28 was removed from this comparison, as the AMS toolkit automatically sets it as identical to *m/z* 44 so does not yield an actual measurement of an organic mass fragment.

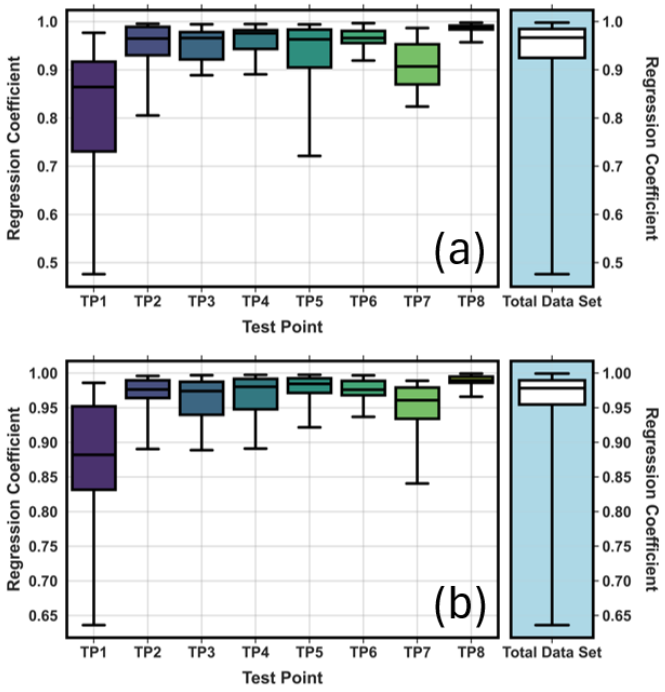

Figure 6. (**a**): Boxplot of ordinary least squares linear regression performed on organic mass concentration produced at each *m/z* (up to *m/z* 150, excluding *m/z* 28) by a fuel at a given condition, compared against the equivalent *m/z* of the organic vPM emitted by another fuel at the same operating condition, above the threshold of 0.5 $\mu g/m^3$. Boxes show interquartile ranges, with median line at centre. Error bars show top and bottom quartiles of the dataset. (**b**): The same as (**a**) except *m/z* 12, 18, 28 and 44 were removed from comparisons.

The mean average regression score was 0.95 with a standard deviation of 0.06. When the organic threshold was raised, the average regression coefficient rose, and the standard

deviation of this decreased. This implies that PM was more compositionally similar at higher concentrations.

The regression coefficients are shown in Figure 6. Figure 6a shows the coefficients for all peaks and Figure 6b shows without *m/z* 12, 18 and 44 (the largest gas contamination peaks) for comparison to remove any potential bias not captured by the filter corrections.

To further examine the vPM's composition, the organic data were analysed with PMF to investigate the possibility of multiple chemical factors being present in the mass spectra, and ultimately a two-factor solution was chosen. These factors consisted of an Alkane factor (AlkOA) and a Quenched Organic Aerosol (QOA), following the terminology of Smith et al., (2022) [25]. The mass spectra of these factors are shown in Figure 7. AlkOA was named as such due to its characteristic alkane fragmentation pattern which is well-established in mass spectrometry literature [25,31,32], though this name does not indicate this is entirely alkane in composition. In short, this consists of a pair of ion series at $C_nH_{2n+1}^+$ and less commonly at C_nH_{2n-1}. These are named the $\Delta = 0$ and 2 series by McLafferty and Turecek (1993) [32]. The QOA factor observed here was also observed by Smith et al. (2022) [25]. The spectral masses of each were taken and plotted against each other in Figure S8 and have a strong correlation ($R^2 = 0.84$). It was observed in vPM also emitted from a different RQL combustor rig used in Smith et al. (2022) [25] but was not observed on a full turboshaft engine examined in the same study. It was hypothesised by the authors that the factor formed due to the rig's quench air, which appeared to oxidise the aerosol, which may be consistent with quenching in the secondary zone of the combustor rig used in this study also.

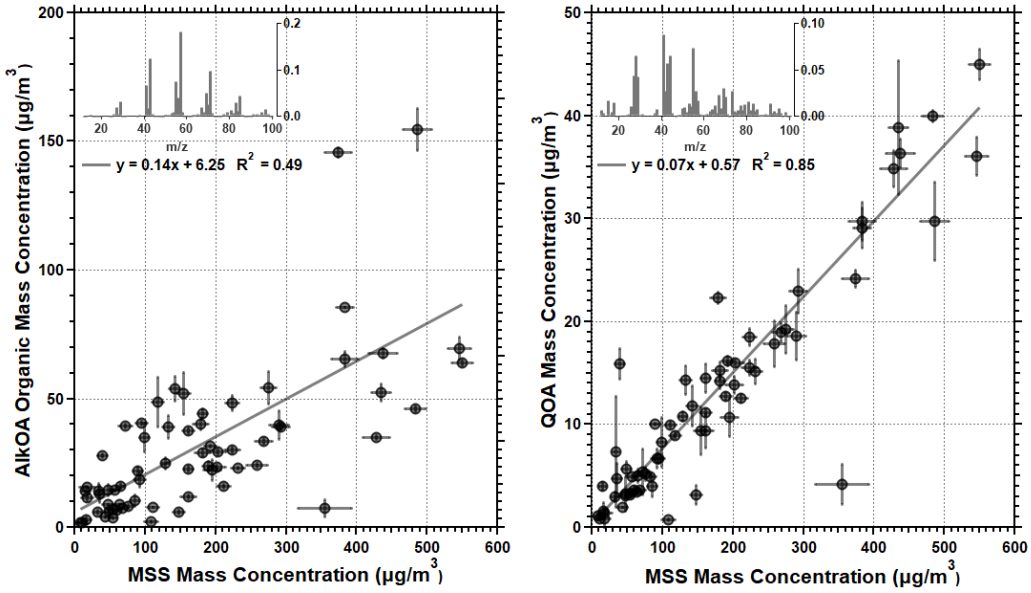

Figure 7. PMF factors and their mass concentrations as a function of MSS EC mass concentration. AlkOA (**left**) and QOA (**right**). Shaded by the hydrogen content of the fuel in the given example.

The use of a high-resolution AMS allows a more detailed examination of the ions contributing to the PMF factors. Ion masses which contributed <1% to the total mass spectrum of each factor were assumed to be noise and not examined with HR analysis. The only exception to this was an aromatic ion series (*m/z* 77, 91, 105, 115 and 128) which was included due to their physical stability. Like the unit mass resolution data already presented, gas phase artifacts were removed using filter data. The masses were compared against the mass spectrometry literature [32,33] and each ion was categorised into one of the following: C_nH_{2n-1}, C_nH_{2n}, C_nH_{2n+1}, aromatic, oxygenated and organosilicon. Any ions which could not be attributed to one of these categories against the mass spectrometry literature was listed under 'unidentified'.

The results of the HR analysis are presented in Figure 8. The AlkOA's largest component was the C_nH_{2n+1} ion series, the second was the C_nH_{2n-1} ion series and the third was the C_nH_{2n} series. The C_nH_{2n+1} and smaller C_nH_{2n-1} are consistent with the fragmentation pattern of alkanes, while C_nH_{2n-1} and C_nH_{2n} is consistent with those of alkenes [32]. QOA had a large reduction in those in the C_nH_{2n+1} category relative to those of the AlkOA factor. This implies that there was a relative reduction in mass contribution of alkane ions in the QOA factor. There was an increase in the C_nH_{2n-1} ions which implies a greater proportion of alkenes [33]. The aromatic ion series in the QOA mass spectrum was six times larger proportionally speaking than AlkOA's. Additionally, 12% of the factor's total mass was also composed of several oxygenated ions.

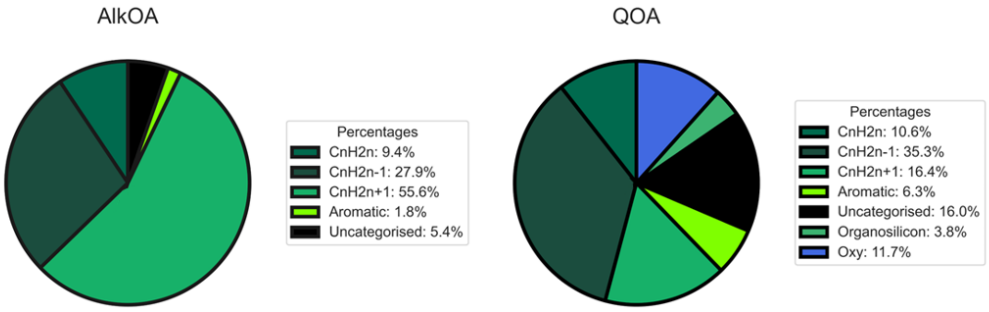

Figure 8. PMF factors, categorised by their AMS ions detected via high-resolution analysis.

Both factors correlated with EC mass (Figure 7). QOA correlated more strongly (R^2 = 0.91) than AlkOA (R^2 = 0.54). As it correlated with EC mass, few trends in QOA's mass concentrations as a function of operating condition were visible.

4. Discussion

Figure 3A,B show, respectively, the total particle number concentrations increasing with EC and with EC combined with either organics (AMS) or OC (OCEC Analyser, represented as TC). This implies that that total number concentrations were dominated by nvPM and that the detected vPM is condensed/agglomerated onto the soot mode.

Hydrogen content provided the strongest correlation of any of the fuel compositional metrics observed, and monoaromatics and cycloalkanes did not vary independently with hydrogen content. With the exception of TP1, diaromatics had a greater correlation than monoaromatics with number concentrations at each test point. The importance of diaromatics in relation to particle number concentrations matches observations in prior studies which have observed trends in particle number concentrations and naphthalene content [10,16]. It should be acknowledged that Brem et al. (2015) [10] noted that the use of hydrogen content reduced naphthalene's observed effect, while the authors also noted contradicting results from Moore et al. (2015) [16], who stated it was a driving factor behind nvPM number concentrations. However, correlation is not causation, and this study cannot fully discriminate between the fuel properties and their impact on emissions, and the effects those might have on the other physical properties of the combustion process and hence observed particle concentrations. For example, in their review of the prior literature, Yang, Boehman and Santoro (2007) [34] noted the differentiation in smoke point difference between mono and diaromatics. This also matched observations stating that fuels with two aromatic rings have greater sooting propensity than those with one [35]. The sooting propensity of diaromatics may explain the results seen here. For example, when averaged across all conditions (TP1–3 and 6–7), J-HA produced 37% higher total particle number concentrations than A-HA, despite J-HA having higher hydrogen content (13.65% compared to A-HA's 13.51%). J-HA had lower aromatics, cycloalkanes and viscosity and comparable molecular weight to A-HA (162 g/mol compared to A-HA's 159 g/mol) yet produced greater particle concentrations. The only fuel parameter (of those presumed here to likely have had such an effect) which J-HA was higher in was diaromatic content.

This observation may explain why J-HA, which has lower hydrogen content than A-HA, produced a greater total number concentration, as J-HA had 2.18% diaromatic content compared to A-HA's 0.28%.

The A-LA fuel had zero aromatics and cycloalkanes yet had a comparable average particle number concentration to B-HE2, which had 12.7% monoaromatic content and 24.5% cycloalkane content. This may appear counterintuitive when compared against results within the existing literature, where hydrogen or aromatic content is observed to often determine emission trends. However, B-HE2 had a lower molecular weight and viscosity, and this may have explained the difference. It is hypothesised here that the discrepancy was caused by molecular weight, despite it having no correlation with particle number concentrations on TP1–7 and only having a low correlation on TP8 (R^2 = 0.3). This low correlation may be due to the class of compound having a greater importance in the determination of the smoke point of a given fuel. Li and Sunderland (2012) [35] reported sooting propensity increasing in the following order: alkanes < alkenes < 1-alkynes < aromatics. Calcote and Manos (1983) [36] noted a similar order, but with napthalenes as the highest. Schalla and McDonald (1953) [37] reported the smoke-free fuel flow of different compound classes in the increasing order aromatics < alkynes < cycloalkanes < isoalkanes < alkanes. However, within a given compounds class, the molecular weight—in the cases of aromatics and n-paraffins—is inversely correlated with smoke point (Hunt, 1953; Schalla and McDonald, 1953) [37]. Calcote and Manos (1983) [36] observed that as fuel molecular weight increases, the flame height in a diffusion flame increases, as more oxygen is required to diffuse into the flame to consume a unit of fuel. It is hypothesised here that the lower molecular weight in B-HE2 relative to A-LA allowed for a higher smoke point in A-LA, and/or the lower viscosity of B-HE2 resulted in better atomisation in the combustor and that one or both of these explain the same total number concentrations produced by these two fuels despite their difference in hydrogen content. Fuel viscosity impacting atomisation, has been previously hypothesised in testing with air blast atomisers [38]. Harper et al., 2022 [9] found, using existing empirical predictions, that the viscosity of many of the fuels examined here were predicted to result in small changes in atomisation properties, although at the current time of writing this has not been experimentally corroborated in relation to the subsequent impact on combustion emissions. This all highlights the need for more research on the impacts of fuel properties.

A lack of sulphate was observed for all fuels and conditions. This may have been because the ranges of sulphur content used here were narrow and low (0–200 ppm). Studies have shown varying fuel sulphur from 383 to 1595 ppm to produce higher sulphate in AMS-detected PM mass concentrations [14,39]. This also may have been due to the combustor exit sampling conditions used here. The gas temperatures operating closely to the rig are higher than those downstream where sulphate has been seen in exhaust plumes (10–30 m). Therefore, the low sulphur content of the fuels examined and/or the higher temperatures may have reduced the formation potential of sulphate vPM, although any nucleation mode aerosols are unlikely to be detected by the AMS, given its 30 nm lower counting threshold.

AMS organics correlated with MSS EC mass concentrations. This indicates that the organics existed as condensed material on a soot surface, which is well documented in the literature [14,25,40]. However, it cannot be ruled out that it was also agglomerated material from a smaller nucleation mode.

Correlation analysis of the mass spectra, and additional PMF and high-resolution analysis, showed that there was almost no (mean average R^2 = 0.96, with peaks *m/z* 12, 18, 28, 44 removed) variation in composition across all fuels and conditions. This was possibly due to the close distances used here, which will have had high exhaust gas temperatures, inhibiting plume evolution, or that fuel composition has no impact on the organic vPM. Some studies have shown little effect of fuel composition on the amount of organic gases [41] and vPM mass [39]. The only possibility for compositional differences in this dataset was at TP1, in which some comparisons had moderate (R^2 ranging from 0.64 to 0.84 in the bottom quartile) correlations, even with potential gas peaks removed.

One comparison showed a different mass spectrum (Figure S9) indicating a different aerosol composition, though one of the conditions involved had half a microgram of organic mass total (so was at the edge of the threshold), and no other such differences appeared in the rest of the dataset. Therefore, the evidence here for fuel composition affecting the emitted aerosol composition is weak. Future studies should examine fuel compositional relationships to organic vPM mass concentrations and composition at greater distances than those applied here.

Very few studies have investigated how fuel composition affects the composition of the consequently emitted vPM. The only paper known to the authors, at the time of writing, is Williams et al., 2012 [42]. There, the researchers examined four alternative aviation fuels and the organic composition of the particulate matter at the exit plane and at ten-meter distance. They found that, in conditions with greater than 10 $\mu g/m^3$, differences in the composition of the PM were observed as the engine power decreased to idle and measurements were made closer to the exit plane, thus differing from the results here. At low power, where the data were above detection limit for the fuels, they observed that the fragmentation of the vPM produced by the alternative fuels was different to the Jet A-1, with R^2 from 0.53 to 0.66. A potentially similar result could be found here in the comparisons between four of the fuels (F4, F7, F5, F8) and J-HA at TP1, which ranged from 0.64 to 0.83 with *m/z* 12, 18, 28 and 44 removed. However, all other comparisons correlated much more strongly than those mentioned by Williams et al. The difference in observations reported here and by Williams et al. could have been due to multiple variables: different engine technologies applied, different fuel compositions, or because fuel has limited relationship to organic PM composition. This indicates more research is needed on this relationship.

Despite the conclusion that fuel had little or no effect on composition, the composition of the organic aerosol was analysed further to examine if it was made up of multiple chemical factors which scaled approximately with one another, which the linear regression analysis would not observe. Further compositional analysis was performed with PMF to achieve this. The observed QOA factor in this RQL combustor helps validate previous observations [25], and how this differing composition from new combustion technologies will alter health impacts warrants further research.

The observation here of oxygenated ions was also implied in the similar factor detected by Smith et al., (2022) [25] due to the presence of a high ratio of *m/z* 44 to 43 (known as $f44/43$ in the aerosol science literature). The observation is also validated here with more precise HR identification of ions. The oxygenated fraction of the QOA factor was of CO_2^+ and H_2O^+ ions. CO_2^+ and H_2O^+ ions have been shown to be present in AMS mass spectra as a result of highly oxygenated organic acids undergoing thermal decarboxylation [43]. H_2O^+ ions can also be symptomatic of alcohols [33], though this can be caused by desorption or an impurity [32]. H_2O^+ ions could have contributions from both gas and aerosol-phase water. Here, gas-phase water has been approximated with filter measurements of H_2O^+ ions and subtracted for each condition. However, the contribution of condensed water in the PM phase cannot be fully accounted for. Despite this uncertainty, the process of thermal decarboxylation of oxo-, di- and polycarboxylic acids to yield a CO_2^+ ion is well replicated in the organic aerosol literature [32,43–45]. Observations over several datasets have noted an indication that atmospheric oxidation converges toward highly aged low-volatility oxygenated organic aerosol (LV-OOA) regardless of the OA source [46]. Kiliç et al., (2018) [23] noted with increasing simulation of ageing of gas turbine gas emissions, using a potential aerosol mass chamber, that the contributions of only carboxylic acids increased. Both the AlkOA and QOA factors observed here correlated with the EC mass concentrations. This may have been due to the proximity to the combustor exit. Future research should aim to examine the effect of fuel composition on this chemical factor by conducting similar experiments at further distances from engine exit.

5. Conclusions

This paper has examined changing aerosol properties as a function of changing fuel characteristics, using an open-source design combustor rig. In line with previous research, hydrogen content was the single variable which correlated most strongly with total particle number concentrations and nvPM mass concentrations. Diaromatic content, viscosity and molecular weight were hypothesised to explain some of the discrepancies in particle number and mass concentrations which could not be explained with hydrogen content alone, and additional influences of fuel properties on other physical processes involved in the combustion process have been proposed. This provides a roadmap for future research to fully explain the observed emissions. The composition of the organic vPM was analysed and, unlike previous studies, showed very little variation as a function of fuel composition at all rig conditions examined. However, by combining the PMF analysis with high-resolution analysis, new insight into the detailed elemental composition of fuel-generated vPM has been revealed. The detection of a QOA factor emitted from an RQL rig has been replicated for the first time, suggesting this is a feature of development rigs with quench air. This study, with the lack of variability in the vPM composition and the confirmed QOA factor, highlights two differences between developmental rigs and full engine emissions. Any changes to engine designs to reduce the impact of PM emissions is conducted at the developmental stage. It is therefore vital these differences are understood so rigs can be used to accurately estimate the impacts once combustors are integrated into full engines. Additionally, future tests should include fuels where their cycloalkane content and monoaromatics vary independently to examine their relationships to the emitted PM. Future studies should also examine how the emerging SAFs affect the vPM and its composition at a greater distance from the aviation source and how fundamental fuel properties impact the combustion process and emitted combustion by-products.

Supplementary Materials: The following supporting information can be downloaded at: https://www.mdpi.com/article/10.3390/atmos15030308/s1, Table S1.—The edited NIOSH 5040 protocol temperature profile for this study; Figure S1. (a) Intercomparison between both CPCs used during this campaign. X-Axis shows concentrations from the CPC used for total number in this testing, y-axis shows the concentrations from the SMPS' CPC. Concentrations were from nebulized sodium chloride particles, which were ran through a DMS, thus selecting for a given size. (b) Comparison between the CPC's number concentration while in single count mode (Number concentrations below 3e5) and SMPS total number concentrations. Please note values in plot b are not diluted corrected as they're intended for instrument comparison purposes only; Figure S2. SMPS size distributions of every test point taken on each fuel. All y-axes were kept consistent to ensure comparability. Shading around test point 8 shows two standard deviations, as multiple SMPS scans were taken. Other test points involved only a single scan; Figure S3. Pika vs Squirrel AMS *m/z* fits; Figure S4. Average residual of high-resolution AMS fits of each *m/z*; Figure S5. Comparison of the effect of varying fuel flow rate, while all other operating metrics held constant, on SMPS number concentrations (top row: 4a, 4b and 4c) and MSS mass concentrations (bottom row: 4d, 4e and 4f) as a function of fuel hydrogen content. Regression values are results of linear regression with the natural log of displayed y values. X-axis error bars show one standard deviation of fuel's repeatability of their compositional analysis. Y-axis error bars in 4d, 4e and 4f show one standard deviation of MSS averages for a given condition. Note, no error bars are shown in 4a, 4b, and 4c as SMPS was only able to take one size range scan for the listed conditions: Table S2. Average particle number change (F_x − J-REF)/J-REF) at a given fuel flow relative to J-REF (Jet A1). Note: values are averaged when fuel flow is held constant while other variables are changing. Fuels are ordered by hydrogen content (% of fuel's mass) from lowest (left) to highest (right) and are displayed below their names, with one standard deviation of its hydrogen content measurement displayed. A 0.6 g/s value is not included for J-LA due to an instrument failure on its TP8: Table S3. Average particle mass concentration reductions (F_x − J-REF)/J-REF) at a given fuel flow relative to J-REF (Jet A1). Note: values are averaged when fuel flow is held constant while other variables are changing. Fuels are ordered by hydrogen content (% of fuel's mass) from lowest (left) to highest (right) and are displayed below their names with one standard deviation of its hydrogen content measurement displayed: Figure S6. AMS organic mass concentrations versus

MSS EC mass concentrations. Out of seventy-four, four AMS results were removed from this due to negative values or highly anomalous results; Table S4. Organic thresholds placed on the data examined with the ordinary least squares linear regression analysis. These regressions were ran on all *m/z* up to 150 with the exception of *m/z* 28 as this is set as identical to *m/z* 44 in the AMS toolkit and therefore does not present a relevant mass fragment. Please note: the organic thresholds provided are for raw measurements, not dilution corrected measurements. This is to enable the use of the instrument's limit of detection as a starting point; Figure S7. OCEC Analyser's OC mass concentrations versus its EC mass concentrations. One test point (B-REF's test point 8) was removed as its OC was highly anomalous (1,388 μ/m^3); Figure S8. Comparisons of the QOA factors observed in this study and by Smith et al (2022) [25]; Figure S9. Mass spectral comparison between J-HA TP1 and A-HA TP1 (above) and its scatter plot (below) with the masses *m/z* 12, 18, 28 and 44 removed; Figure S10. SMPS Number vs fuel properties; Figure S11. MSS concentration vs fuel properties.

Author Contributions: Conceptualisation: M.J. and A.C.; Methodology: P.I.W., M.J., A.C. and L.D.S.; Software: L.D.S. and P.I.W.; Validation: L.D.S. and P.I.W.; Formal Analysis: J.H. (Fuel Compositional Analysis), L.D.S. (Everything else); Writing—original draft preparation: L.D.S.; Writing—review and editing: L.D.S., P.I.W., E.D., J.H., M.J., A.C. and H.C.; Visualisation: L.D.S.; Supervision: P.I.W.; Project Administration: M.J. All authors have read and agreed to the published version of the manuscript.

Funding: This research was funded by the Natural Environment Research Council (NERC) EAO Doctoral Training Partnership, grant reference number NE/R009732/1, and Rolls-Royce plc, whose support is gratefully acknowledged.

Institutional Review Board Statement: Not applicable.

Informed Consent Statement: Not applicable.

Data Availability Statement: The data presented in this study are available on request from the corresponding author. The data are not publicly available due not being archived on a public server.

Acknowledgments: This work was supported by the National Centre for Atmospheric Science (NCAS) through use of equipment from the Atmospheric Measurement and Observation Facility (AMOF). This work acknowledges the support of the FLITES and JETScreen projects, as well as EASA for the use of the European reference system. Thanks is given for the support of the GTRC and staff.

Conflicts of Interest: The research was funded by Rolls-Royce plc, and coauthor Mark Johnson supervised the main author Liam D. Smith. At no point did any representative of Rolls-Royce plc suggest that the data or results be manipulated in an unethical manner.

References

1. Grewe, V.; Rao, A.G.; Grönstedt, T.; Xisto, C.; Linke, F.; Melkert, J.; Middel, J.; Ohlenforst, B.; Blakey, S.; Christie, S.; et al. Evaluating the climate impact of aviation emission scenarios towards the Paris agreement including COVID-19 effects. *Nat. Commun.* **2021**, *12*, 3841. [CrossRef] [PubMed]
2. Lee, D.S.; Fahey, D.W.; Forster, P.M.; Newton, P.J.; Wit, R.C.N.; Lim, L.L.; Owen, B.; Sausen, R. Aviation and global climate change in the 21st century. *Atmos. Environ.* **2009**, *43*, 3520–3537. [CrossRef] [PubMed]
3. Lee, D.; Pitari, G.; Grewe, V.; Gierens, K.; Penner, J.; Petzold, A.; Prather, M.; Schumann, U.; Bais, A.; Berntsen, T.; et al. Transport impacts on atmosphere and climate: Aviation. *Atmos. Environ.* **2010**, *44*, 4678–4734. [CrossRef] [PubMed]
4. Hudda, N.; Fruin, S.A. International Airport Impacts to Air Quality: Size and Related Properties of Large Increases in Ultrafine Particle Number Concentrations. *Environ. Sci. Technol.* **2016**, *50*, 3362–3370. [CrossRef] [PubMed]
5. Hudda, N.; Gould, T.; Hartin, K.; Larson, T.V.; Fruin, S.A. Emissions from an international airport increase particle number concentrations 4-fold at 10 km downwind. *Environ. Sci. Technol.* **2014**, *48*, 6628–6635. [CrossRef] [PubMed]
6. Yim, S.H.; Stettler, M.E.; Barrett, S.R. Air quality and public health impacts of UK airports. Part II: Impacts and policy assessment. *Atmos. Environ.* **2013**, *67*, 184–192. [CrossRef]
7. He, R.-W.; Shirmohammadi, F.; Gerlofs-Nijland, M.E.; Sioutas, C.; Cassee, F.R. Pro-inflammatory responses to PM0.25 from airport and urban traffic emissions. *Sci. Total Environ.* **2018**, *640–641*, 997–1003. [CrossRef]
8. Yu, Z.; Herndon, S.C.; Ziemba, L.D.; Timko, M.T.; Liscinsky, D.S.; Anderson, B.E.; Miake-Lye, R.C. Identification of lubrication oil in the particulate matter emissions from engine exhaust of in-service commercial aircraft. *Environ. Sci. Technol.* **2012**, *46*, 9630–9637. [CrossRef]
9. Harper, J.; Durand, E.; Bowen, P.; Pugh, D.; Johnson, M.; Crayford, A. Influence of alternative fuel properties and combustor operating conditions on the nvPM and gaseous emissions produced by a small-scale RQL combustor. *Fuel* **2022**, *315*, 123045. [CrossRef]

10. Brem, B.T.; Durdina, L.; Siegerist, F.; Beyerle, P.; Bruderer, K.; Rindlisbacher, T.; Rocci-Denis, S.; Andac, M.G.; Zelina, J.; Penanhoat, O.; et al. Effects of Fuel Aromatic Content on Nonvolatile Particulate Emissions of an In-Production Aircraft Gas Turbine. *Environ. Sci. Technol.* **2015**, *49*, 13149–13157. [CrossRef]
11. Chan, T.W.; Canteenwalla, P.; Chishty, W.A. Characterization of fuel composition and altitude impact on gaseous and particle emissions from a turbojet engine. In Proceedings of the ASME Turbo Expo 2017: Turbomachinery Technical Conference and Exposition, Charlotte, NC, USA, 26–30 June 2017.
12. Tran, S.; Brown, A.; Olfert, J.S. Comparison of Particle Number Emissions from In-Flight Aircraft Fueled with Jet A1, JP-5 and an Alcohol-to-Jet Fuel Blend. *Energy Fuels* **2020**, *34*, 7218–7222. [CrossRef]
13. Beyersdorf, A.; Timko, M.; Ziemba, L.; Bulzan, D.; Corporan, E.; Herndon, S.; Howard, R.; Miake-Lye, R.; Thornhill, K.; Winstead, E. Reductions in aircraft particulate emissions due to the use of Fischer–Tropsch fuels. *Atmos. Chem. Phys.* **2014**, *14*, 11–23. [CrossRef]
14. Onasch, T.B.; Jayne, J.T.; Herndon, S.; Worsnop, D.R.; Miake-Lye, R.C.; Mortimer, I.P.; Anderson, B.E. Chemical Properties of Aircraft Engine Particulate Exhaust Emissions. *J. Propuls. Power* **2009**, *25*, 1121–1137. [CrossRef]
15. Miake-Lye, R.C.; Anderson, B.E.; Cofer, W.R.; Wallio, H.A.; Nowicki, G.D.; Ballenthin, J.O.; Hunton, D.E.; Knighton, W.B.; Miller, T.M.; Seeley, J.V.; et al. SO_x oxidation and volatile aerosol in aircraft exhaust plumes depend on fuel sulfur content. *Geophys. Res. Lett.* **1998**, *25*, 1677–1680. [CrossRef]
16. Moore, R.H.; Shook, M.; Beyersdorf, A.; Corr, C.; Herndon, S.; Knighton, W.B.; Miake-Lye, R.; Thornhill, K.L.; Winstead, E.L.; Yu, Z.; et al. Influence of jet fuel composition on aircraft engine emissions: A synthesis of aerosol emissions data from the NASA APEX, AAFEX, and ACCESS missions. *Energy Fuels* **2015**, *29*, 2591–2600. [CrossRef]
17. Anderson, B.E.; Cofer, W.R.; Barrick, J.D.; Bagwell, D.R.; Hudgins, C.H. Airborne observations of aircraft aerosol emissions II: Factors controlling volatile particle production. *Geophys. Res. Lett.* **1998**, *25*, 1693–1696. [CrossRef]
18. Timko, M.T.; Fortner, E.; Franklin, J.; Yu, Z.; Wong, H.-W.; Onasch, T.B.; Miake-Lye, R.C.; Herndon, S.C. Atmospheric measurements of the physical evolution of aircraft exhaust plumes. *Environ. Sci. Technol.* **2013**, *47*, 3513–3520. [CrossRef]
19. Wey, C.C.; Anderson, B.E.; Wey, C.; Miake-Lye, R.C.; Whitefield, P.; Howard, R. Overview on the aircraft particle emissions experiment. *J. Propuls. Power* **2007**, *23*, 898–904. [CrossRef]
20. Bulzan, D.; Anderson, B.; Wey, C.; Howard, R.; Winstead, E.; Beyersdorf, A.; Corporan, E.; DeWitt, M.I.; Klingshirn, C.; Herndon, S. Gaseous and particulate emissions results of the NASA alternative aviation fuel experiment (AAFEX). In Proceedings of the ASME Turbo Expo 2010: Power for Land, Sea, and Air, Glasgow, UK, 14–18 June 2010. GT2010–23524.
21. Anderson, B. Alternative Aviation Fuel Experiment II (AAFEX II) Overview. In Proceedings of the 3rd International Conference on Transport, Atmosphere and Climate, Prien am Chiemsee, Germany, 25–28 June 2012.
22. Lobo, P.; Durdina, L.; Smallwood, G.J.; Rindlisbacher, T.; Siegerist, F.; Black, E.A.; Yu, Z.; Mensah, A.A.; Hagen, D.E.; Miake-Lye, R.C.; et al. Measurement of aircraft engine non-volatile PM emissions: Results of the Aviation-Particle Regulatory Instrumentation Demonstration Experiment (A-PRIDE) 4 campaign. *Aerosol Sci. Technol.* **2015**, *49*, 472–484. [CrossRef]
23. Kılıç, D.; El Haddad, I.; Brem, B.T.; Bruns, E.; Bozetti, C.; Corbin, J.; Durdina, L.; Huang, R.-J.; Jiang, J.; Klein, F.; et al. Identification of secondary aerosol precursors emitted by an aircraft turbofan. *Atmos. Chem. Phys.* **2018**, *18*, 7379–7391. [CrossRef]
24. Lobo, P.; Durdina, L.; Brem, B.T.; Crayford, A.P.; Johnson, M.P.; Smallwood, G.J.; Siegerist, F.; Williams, P.I.; Black, E.A.; Llamedo, A.; et al. Comparison of standardized sampling and measurement reference systems for aircraft engine non-volatile particulate matter emissions. *J. Aerosol Sci.* **2020**, *145*, 105557. [CrossRef]
25. Smith, L.D.; Allan, J.; Coe, H.; Reyes-Villegas, E.; Johnson, M.P.; Crayford, A.; Durand, E.; Williams, P.I. Examining chemical composition of gas turbine-emitted organic aerosol using positive matrix factorization (PMF). *J. Aerosol Sci.* **2021**, *159*, 105869. [CrossRef]
26. Makida, M.; Yamada, H.; Kurosawa, Y.; Yamamoto, T.; Matsuura, K.; Hayashi, S. Preliminary Experimental Research to Develop a Combustor for Small Class Aircraft Engine Utilizing Primary Rich Com-bustion Approach. In Proceedings of the ASME Turbo Expo 2006: Power for Land, Sea and Air, Barcelona, Spain, 8–11 May 2006; pp. 1–8.
27. Crayford, A.P.; Lacan, F.; Runyon, J.; Bowen, P.J.; Balwadkar, S.; Harper, J.; Pugh, D.G. Manufacture, Characterization and Stability Limits of an Am Prefilming Air-Blast Atomizer. In Proceedings of the ASME Turbo Expo 2019: Turbomachinery Technical Conference and Exposition, Phoenix, AZ, USA, 17–21 June 2019; American Society Mechanical Engineers: New York, NY, USA, 2019.
28. ICAO. *Annex 16—Environmental Protection*; ICAO: Montreal, QC, Canada, 2018; Volume 2.
29. Petzold, A.; Marsh, R.; Johnson, M.; Miller, M.; Sevcenco, Y.; Delhaye, D.; Ibrahim, A.; Williams, P.; Bauer, H.; Crayford, A.; et al. Evaluation of methods for measuring particulate matter emissions from gas turbines. *Environ. Sci. Technol.* **2011**, *45*, 3562–3568. [CrossRef] [PubMed]
30. Durand, E.; Durdina, L.; Smallwood, G.; Johnson, M.; Spirig, C.; Edebeli, J.; Roth, M.; Brem, B.; Sevcenco, Y.; Crayford, A. Correction for particle loss in a regulatory aviation nvPM emissions system using measured particle size. *J. Aerosol Sci.* **2023**, *169*, 106140. [CrossRef]
31. Timko, M.T.; Albo, S.E.; Onasch, T.B.; Fortner, E.C.; Yu, Z.; Miake-Lye, R.C.; Canagaratna, M.R.; Ng, N.L.; Worsnop, D.R. Composition and sources of the organic particle emissions from aircraft engines. *Aerosol Sci. Technol.* **2014**, *48*, 61–73. [CrossRef]
32. McLafferty, F.; Turecek, F.W. *Interpretation of Mass Spectra*, 4th ed.; University Science Books: Sausalito, CA, USA, 1993.
33. McCullagh, N.; Oldham, J. *Mass Spectrometry*; Oxford University Press: Oxford, UK, 2019.

34. Yang, Y.; Boehman, A.L.; Santoro, R.J. A study of jet fuel sooting tendency using the threshold sooting index (TSI) model. *Combust. Flame* **2007**, *149*, 191–205. [CrossRef]
35. Li, L.; Sunderland, P.B. An improved method of smoke point normalization. *Combust. Sci. Technol.* **2012**, *184*, 829–841. [CrossRef]
36. Calcote, H.; Manos, D. Effect of molecular structure on incipient soot formation. *Combust. Flame* **1983**, *49*, 289–304. [CrossRef]
37. Schalla, R.L.; McDonald, G.E. Variation in Smoking Tendency. *Ind. Eng. Chem.* **1953**, *53*, 1497–1500. [CrossRef]
38. Rye, L.; Wilson, C. The influence of alternative fuel composition on gas turbine ignition performance. *Fuel* **2012**, *96*, 277–283. [CrossRef]
39. Onasch, T.B.; Jayne, J.T.; Herndon, S.C.; Mortimer, P.; Worsnop, D.R.; Miake-lye, R.C. Aircraft Particle Emissions eX-periment (APEX): Chemical Properties of Aircraft Engine Exhaust Aerosols Sampled During APEX (Appendix J). In *Aircraft Particle Emissions eXperiment (APEX)—NASA/TM—2006-214382*; NASA: Washington, DC, USA, 2006; pp. 475–500.
40. Timko, M.T.; Onasch, T.B.; Northway, M.J.; Jayne, J.T.; Canagaratna, M.R.; Herndon, S.C.; Wood, E.C.; Miake-Lye, R.C.; Knighton, W.B. Gas turbine engine emissions—Part II: Chemical properties of particulate matter. *J. Eng. Gas Turbines Power* **2010**, *132*, 061505. [CrossRef]
41. Yelvington, P.E.; Herndon, S.C.; Wormhoudt, J.C.; Jayne, J.T.; Miake-Lye, R.C.; Knighton, W.B.; Wey, C. Chemical Speciation of Hydrocarbon Emissions from a Commercial Aircraft Engine. *J. Propuls. Power* **2007**, *23*, 912–918. [CrossRef]
42. Williams, P.I.; Allan, J.D.; Lobo, P.; Coe, H.; Christie, S.; Wilson, C.; Hagen, D.; Whitefield, P.; Raper, D.; Rye, L. Impact of alternative fuels on emissions characteristics of a gas turbine engine—Part 2: Volatile and semivolatile particulate matter emissions. *Environ. Sci. Technol.* **2012**, *46*, 10812–10819. [CrossRef] [PubMed]
43. Alfarra, M. *Insights into Atmospheric Organic Aerosols Using an Aerosol Mass Spectrometer*; University of Manchester: Manchester, UK, 2004.
44. Yu, Z.; Timko, M.T.; Herndon, S.C.; Richard, C.M.-L.; Beyersdorf, A.J.; Ziemba, L.D.; Winstead, E.L.; Anderson, B.E. Mode-specific, semi-volatile chemical composition of particulate matter emissions from a commercial gas turbine aircraft engine. *Atmos. Environ.* **2019**, *218*, 116974. [CrossRef]
45. Ng, N.L.; Canagaratna, M.R.; Zhang, Q.; Jimenez, J.L.; Tian, J.; Ulbrich, I.M.; Kroll, J.H.; Docherty, K.S.; Chhabra, P.S.; Bahreini, R.; et al. Organic aerosol components observed in Northern Hemispheric datasets from Aerosol Mass Spectrometry. *Atmos. Chem. Phys.* **2010**, *10*, 4625–4641. [CrossRef]
46. Rollins, A.W.; Fry, J.L.; Hunter, J.F.; Kroll, J.H.; Worsnop, D.R.; Singaram, S.W.; Cohen, R.C. Elemental analysis of aerosol organic nitrates with electron ionization high-resolution mass spectrometry. *Atmos. Meas. Tech.* **2010**, *3*, 301–310. [CrossRef]